

The mass, luminosity and mass-loss rate of the donor of the V1387 Aql/GRS 1915+105 binary system

Janusz Ziółkowski[★] and Andrzej A. Zdziarski[★]

Nicolaus Copernicus Astronomical Center, Polish Academy of Sciences, Bartycka 18, PL-00-716 Warszawa, Poland

19 June 2019

ABSTRACT

V1387 Aql (the donor in the microquasar GRS 1915+105) is a low-mass giant. Such a star consists of a degenerate helium core and a hydrogen-rich envelope. Both components are separated by an hydrogen burning shell. The structure of such an object is relatively simple and easy to model. Making use of the observational constraints on the luminosity and the radius of V1387 Aql, we constrain the mass of this star with evolutionary models. We find a very good agreement between the constraints from those models and from the observed rotational broadening and the NIR magnitude. Combining the constraints, we find solutions with stripped giants of the mass of $\geq 0.28M_{\odot}$ and of the spectral class K5 III, independent of the distance to the system, and a distance-dependent upper limit, $\lesssim 1M_{\odot}$. We also calculate the average mass transfer rate and the duty cycle of the system as a function of the donor mass.

Key words: binaries: general – stars: evolution – stars: individual: V1387 Aql – X-rays: binaries – X-rays: individual: GRS 1915+105.

1 INTRODUCTION

GRS 1915+105 is a low mass X-ray binary, which appears to be the most distinct Galactic microquasar (Mirabel & Rodríguez 1994). The system contains a black hole and a low mass K–M III giant donor (Greiner et al. 2001b; Harlaftis & Greiner 2004; Steeghs et al. 2013), and it has a long period of $P = 33.85 \pm 0.16$ d (Steeghs et al. 2013). The donor, which got a variable-star name V1387 Aql, fills its Roche lobe and supplies the matter accreted by the black hole. The first determination of the mass of the black hole based on a measurement of the radial velocity amplitude, K_2 , was by Greiner, Cuby & McCaughrean (2001a), who, observing with the VLT, obtained $K_2 = 140 \pm 15$ km s^{−1}. This indicated that the system contains one of the heaviest Galactic black holes with the mass of $M_1 = 14 \pm 4M_{\odot}$ (assuming the binary inclination of $i \approx 70^\circ$ of Mirabel & Rodríguez 1994). This measurement was later refined by Steeghs et al. (2013), who also used the VLT but at a higher spectral resolution, and obtained $K_2 = 126 \pm 1$ km s^{−1}, which, given that $M_1 \propto (K_2/\sin i)^3$, results in a reduction of this mass. The exact value depends on the inclination, which, for GRS 1915+105, is usually determined from the jet kinematics, which, in turn, depends on the distance to the source (Mirabel & Rodríguez 1994; Fender et al. 1999). After the successful radio parallax measurement by Reid et al. (2014), the distance is determined to be $d = 8.6^{+2.0}_{-1.6}$ kpc, which then yields $M_1 = 12.4^{+2.0}_{-1.8}M_{\odot}$ (Reid et al. 2014). This distance determination is consistent with an indepen-

dent estimate of $d \lesssim 10$ kpc by Zdziarski (2014) based on considering the jet kinetic power.

While the mass of the black hole may be now considered as relatively precisely known, it is less so for the mass of the donor. The first rough estimate implied by the spectral classification (K–M III) was proposed by Greiner et al. (2001b) as $M_2 \approx (1.0\text{--}1.5)M_{\odot}$. However, this is a range typical for isolated giants of these classes (Cox 2000), while the donor in GRS 1915+105 could have lost a large fraction of its mass. This has been confirmed by measurements of the rotational broadening. First, Harlaftis & Greiner (2004) found it as $v \sin i = 26 \pm 3$ km s^{−1}. This quantity combined with K_2 yields the binary mass ratio, $q \equiv M_2/M_1$. Harlaftis & Greiner (2004) used the value of K_2 of Greiner et al. (2001a), which yields $q = 0.058 \pm 0.033$. The current best measurement of the rotational broadening is that of Steeghs et al. (2013), $v \sin i = 21 \pm 4$ km s^{−1}. This value combined with their K_2 measurement yields $q \approx 0.042 \pm 0.024$. For the distance-dependent black-hole mass estimate of Reid et al. (2014), this gives $M_2 \approx 0.52 \pm 0.31M_{\odot}$. Thus, the donor has the mass substantially lower than that of an isolated star of the same spectral class, i.e., it is a ‘stripped giant’ (e.g., Webbink, Rappaport & Savonije 1983, hereafter WRS83). We note that Steeghs et al. (2013) gave a rather conservative estimate on the error of $v \sin i$. From the bottom panel of their fig. 4 we would infer a standard deviation of $\lesssim 3$ km s^{−1}, which would translate into a standard deviation of q of $\lesssim 0.017$, and that on the standard deviation of M_2 of $\lesssim 0.23M_{\odot}$. Even then, the uncertainty on the donor mass is rather large.

We explore here another possibility to constrain the donor mass based on modelling of its internal structure. Since the donor

[★] E-mail: jz@camk.edu.pl, aaz@camk.edu.pl

is not a main sequence star but rather an evolved low-mass giant, its structure is relatively simple and easy to model. Making use of the observational constraints on the luminosity and the radius of V1387 Aql, we construct an evolutionary model of this star and attempt to constrain its mass. For that, we also need the effective temperature of the donor. The currently most accurate NIR observations of this system are those of [Steehgs et al. \(2013\)](#), who matched their spectra to those of K0, K1, K2, K5 III and M0 III template stars. Thus, we adopt here the possible range of the spectral classes¹ from K0 III to M0 III.

2 OBSERVATIONALLY DETERMINED PARAMETERS

From the third Kepler law, we have the separation of the components as

$$A = \frac{(GM)^{1/3} P^{2/3}}{(2\pi)^{4/3}} \approx 4.207 R_{\odot} (M/M_{\odot})^{1/3} (P/1 \text{ d})^{2/3}, \quad (1)$$

where $M = M_1 + M_2$ is the total mass. The relation between the radius of the optical component (which must be equal to the radius of its Roche lobe) and the separation of the components for $M_2 \ll M_1$ is ([Paczynski 1967](#))

$$R_2 = \frac{2A}{3^{4/3}} \left(\frac{M_2}{M} \right)^{1/3}. \quad (2)$$

From equations (1–2) we have

$$R_2 = (2GM_2)^{1/3} \left(\frac{P}{9\pi} \right)^{2/3} \approx 1.945 R_{\odot} (M_2/M_{\odot})^{1/3} (P/1 \text{ d})^{2/3}. \quad (3)$$

Let us note that generally equation (3) makes radius of the donor filling its Roche lobe one of the most accurately determined parameters of that star. The orbital period is usually known with the high precision and the dependence on M_2 is weak. Moreover, equation (3) does not depend on the distance to the binary system. For discussion of the accuracy of equation (3) see, e.g., [Zdziarski et al. \(2016\)](#). Given the small uncertainty on the period, its contribution to the error is negligible.

The Roche-lobe radius for a given donor mass of equation (3), $R_2(M_2, P)$, is, in fact, identical to that implied by the rotational broadening,

$$R_2 = \frac{P(v \sin i)}{2\pi \sin i}, \quad (4)$$

for $M_2 = q(v \sin i, K_2) M_1(K_2, P, i, q)$ substituted in the former. Here q follows from the standard rotational-broadening relationship (e.g., [Wade & Horne 1988](#)), which solution can be found as

$$q = \frac{[r(y) - 1]^2}{3r(y)}, \quad r(y) = 2^{-1/3} \left[2 + 27y + 3^{3/2} \sqrt{y(4 + 27y)} \right]^{1/3} \geq 1, \quad (5)$$

$$y = \left(\frac{3^{4/3} v \sin i}{2K_2} \right)^3,$$

while the black-hole mass is

$$M_1 = \frac{PK_2^3(1+q)^2}{2\pi G \sin^3 i}. \quad (6)$$

¹ [Fragos & McClintock \(2015\)](#) gave the range of the spectral class of V1387 Aql as K0–3 III, but that choice was not based on any additional constraints with respect to those of [Steehgs et al. \(2013\)](#) (J. McClintock, private communication.) Also, they gave $M_2 \approx 0.58 \pm 0.33 M_{\odot}$, which appears to be due to a typo.

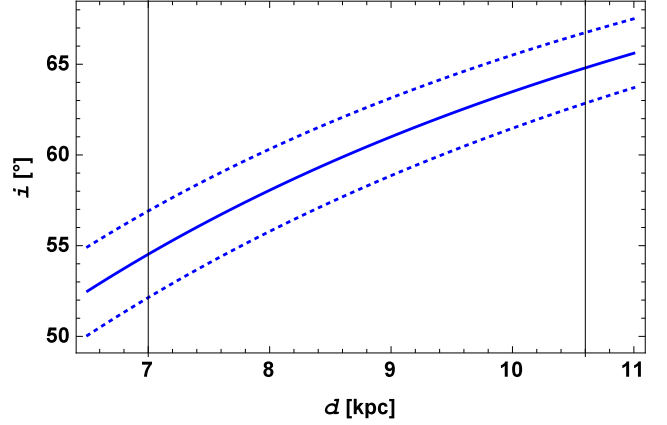


Figure 1. The relationship between the distance and the inner jet inclination based on the observations of [Fender et al. \(1999\)](#). If the jet is aligned with the binary axis, i is also the binary inclination. The solid curve gives the best estimate, and the dotted curves give the range corresponding to the measurement errors. The range of d determined from the radio parallax by [Reid et al. \(2014\)](#) is shown by the vertical thin lines.

Equations (4–5) assume corotation, which is very likely in GRS 1915+105.

We can relate the inclination to the distance by assuming the inner jet has the same direction as the binary axis, which yields $i = \arctan[2\mu_a\mu_r d/(\mu_a - \mu_r)c]$, where μ_a and μ_r are, respectively, the angular velocities of the approaching and receding jet. [Zdziarski \(2014\)](#) used the weighted average of the inclination resulting from the observations by [Mirabel & Rodriguez \(1994\)](#) and [Fender et al. \(1999\)](#). On the other hand, [Reid et al. \(2014\)](#) argued that the jet direction changes between the projected distance from the centre of $0.3''$ (observed by [Fender et al. 1999](#)) and $1''$ ([Mirabel & Rodriguez 1994](#)), and thus the results of the former are more relevant for estimating the binary plane orientation, resulting in $i = 59^{+5}_{-4}^\circ$. We show the $i(d)$ relationship in Fig. 1.

[Steehgs et al. \(2013\)](#) argued that the alignment is very likely, and this assumption has indeed been universally used in the mass estimates for GRS 1915+105. On the other hand, an also likely and widely accepted, model for the low-frequency QPOs/breaks in the power spectra of black-hole binaries is the Lense-Thirring precession of an inner hot part of the accretion flow (e.g., [Ingram, Done & Fragile 2009; Ingram & Done 2011](#)). This model requires a misalignment between the black-hole spin and binary axes, though the minimum required misalignment appears not to be specified. GRS 1915+105 does show low-frequency QPOs (e.g., [Yan et al. 2013](#)), which appear very similar to those in other black-hole binaries, and the above model can apply to it. Also, the black-hole binary GRO J1655–40 has an accurate determination of the orbital axis inclination of $68.65 \pm 1.5^\circ$ ([Beer & Podsiadlowski 2002](#)), which is significantly different from the jet axis inclination of $85 \pm 2^\circ$ ([Hjellming & Rupen 1995](#)). If the axes are different in GRS 1915+105 as well, the alignment-based estimates would become inaccurate, and, e.g., the marked difference between the black-hole mass of GRS 1915+105 of $M_1 = 12.4^{+2.0}_{-1.8} M_{\odot}$ ([Reid et al. 2014](#)) and those typical for accreting low-mass black-hole binaries of $7.8 \pm 1.2 M_{\odot}$ ([Özel et al. 2010](#)) may disappear. (We note here that the above average may need to be updated, e.g., taking into account the revision of the black-hole mass in Nova Muscae from $7.2 \pm 0.7 M_{\odot}$ to $11.0^{+2.1}_{-1.4} M_{\odot}$, [Wu et al. 2016](#).)

Given this uncertainty, we show the constraints on the radius

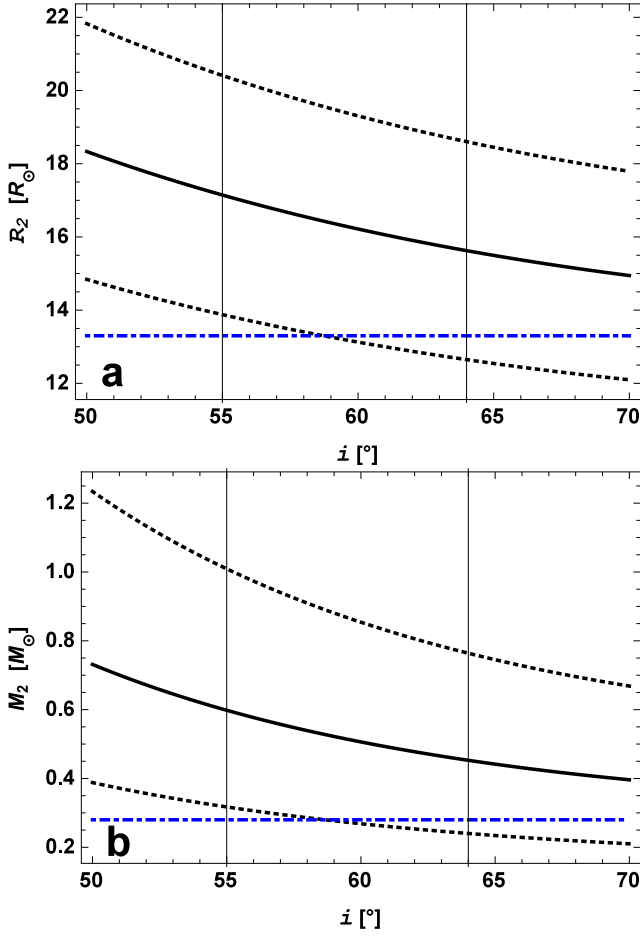


Figure 2. The donor radius (a) and mass (b) as functions of the binary inclination. The black solid curves give the best-fit values from the observed rotational broadening assuming the Roche-lobe filling and corotation, and the black dotted curves enclose the ranges of uncertainties, which is dominated by the measurement error of $v \sin i$. The range of i compatible with the parallax distance, assuming the alignment of the jet with the binary axis, and using the results of Fender et al. (1999) is 55° – 64° (Reid et al. 2014), as shown by the vertical thin lines. The horizontal blue dot-dashed lines show $M_2 = 0.28$ and the corresponding radius, which are the minimum possible values found from evolutionary stellar models in Section 3. The ranges allowed by both the observations and the models are those below the upper dotted curve and above both the dot-dashed and lower dotted curves.

and mass of the donor as functions of both the inclination and the distance, with the latter assuming the alignment. Fig. 2 shows the $R_2(i)$ and $M_2(i)$ dependencies, which do not assume the alignment. We show there, though, the range of the inclinations obtained by Reid et al. (2014) (assuming the alignment). Then, Fig. 3 shows the $R_2(d)$ and $M_2(d)$ dependencies, which assume the alignment.

We can also constrain the size and mass of the donor vs. the distance by using the observed NIR flux of the donor (as first done by Zdziarski et al. 2005). The unveiled donor K magnitude (at $\lambda = 2.2\mu\text{m}$) and the extinction towards the system have been estimated as 14.5–15.0 and 2.2 ± 0.3 by Greiner et al. (2001b) and Chapuis & Corbel (2004), respectively. This gives the extinction-corrected magnitude of K ≈ 12.0 – 13.1 , or the flux per unit wavelength at $2.2\mu\text{m}$ as $(2.2\text{--}6.2) \times 10^{-8} \text{ erg s}^{-1} \text{ cm}^{-3}$. By approximating the stellar spectrum as a blackbody at the effective temperature, $B_\lambda(T_{\text{eff}})$, i.e., $F_\lambda = \pi B_\lambda(T_{\text{eff}})(R_2/d)^2$, we can then obtain the stellar radius as a function of the distance. The results for

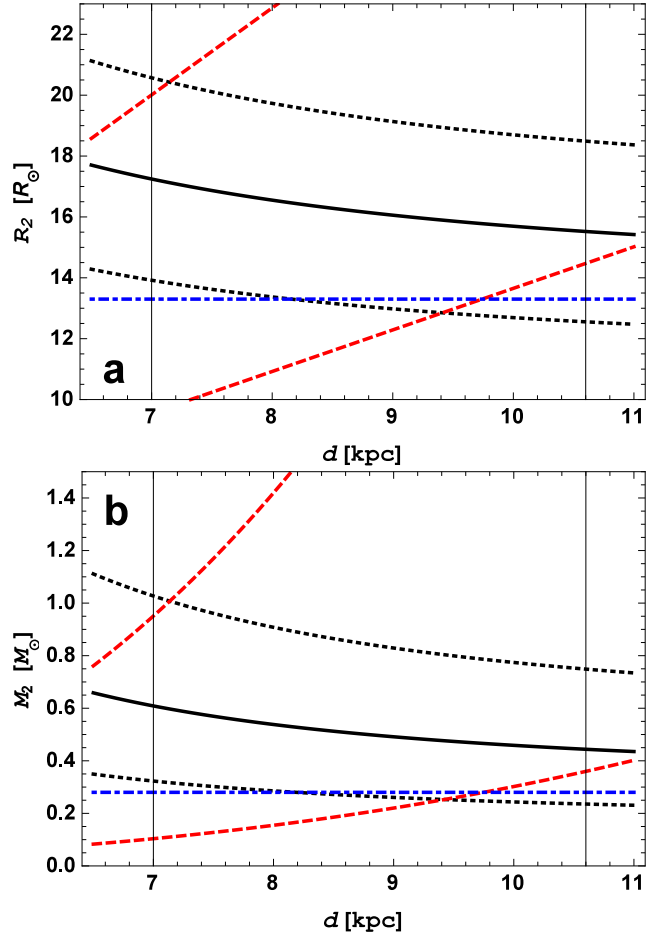


Figure 3. The donor radius (a) and mass (b) as functions of the distance. The black solid curves show the best-fit values from the observed rotational broadening assuming the Roche-lobe filling, corotation and alignment of the jet and binary axes, and the black dotted curves enclose the ranges of uncertainties. The range of d from the parallax (Reid et al. 2014) is shown by the vertical thin lines. The red dashed curves enclose the range allowed by the observed NIR flux (approximately independent of i). The horizontal blue dot-dashed lines show $M_2 = 0.28$ and the corresponding radius, which are the minimum possible values based on evolutionary consideration. The allowed parameter region is within the innermost dotted, dashed and dot-dashed curves and the vertical lines.

the temperatures within the range of $T_{\text{eff}} = 3690$ – 4660 K (Cox 2000), corresponding to the adopted range of the spectral classes of K0 III–M0 III, are shown by the dashed red curves in Fig. 3. These results are basically equivalent, and almost the same as those obtained using the Barnes-Evans relation (Barnes & Evans 1976; Beuermann, Baraffe & Hauschildt 1999), as given for the K magnitude by equation (1a) of Cahn (1980), and for the range of the surface brightness of $F_K = 3.81$ – 3.86 (which approximately corresponds to K0–M0 giants, see fig. 2 of Cahn 1980).

Combining the above constraints for the allowed range of the distance, we find $12.5 \lesssim R_2/R_\odot \lesssim 21$ and $0.25 \lesssim M_2/M_\odot \lesssim 1$. The upper limit is larger than that of Steeghs et al. (2013) because they gave that from propagation of errors, while here we give it for the entire allowed range of d . At a given distance, the constraints are more stringent, as shown on Fig. 3.

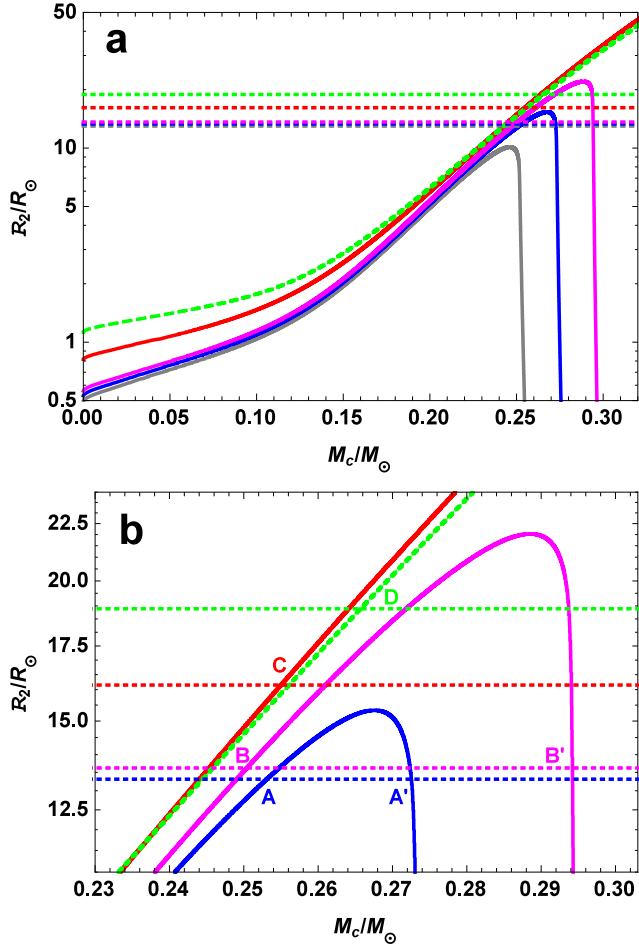


Figure 4. Evolution of partially stripped giants in the M_c – R_2 diagram for $M_2 = 0.26, 0.28, 0.3$ and 0.5 and $0.8M_\odot$ for the grey, blue, magenta, red and green curves, respectively. The evolution proceeds (from left to right) at the constant total mass, during which the H-burning shell is moving outwards. This increases the mass of the He core and decreases the mass of the H-rich envelope. The horizontal lines (in respective colours) show the Roche-lobe radii for (from the top) $M_2 = 0.8, 0.5, 0.3, 0.28$ and $0.26M_\odot$. Possible solutions for V1387 Aql are given by the intersections between a horizontal line and the corresponding evolutionary track. (a) The full studied parameter space. (b) A magnification of the intersection region. The possible solutions are marked with the letters: A and A' for $M_2 = 0.28M_\odot$, B and B' for $0.3M_\odot$, and C and D for 0.5 and $0.8M_\odot$, respectively. The solutions A' and B' are unphysical as they do not assure a continuous mass transfer.

3 THE MODELS OF V1387 Aql

3.1 The core mass–radius plane

In order to calculate evolutionary models of stripped giants, we used the Warsaw stellar-evolution code (described in Ziolkowski 2005). The code was calibrated to reproduce the Sun at the solar age. This calibration resulted in the chemical composition of the H mass fraction of $X = 0.74$, the metallicity of $Z = 0.014$, and the mixing length parameter of $\alpha = 1.55$.

To reproduce the present state of V1387 Aql, we followed the evolution of a $1M_\odot$ star, which was maintained at a constant mass until hydrogen was nearly exhausted in its centre. Then, the mass removal from the surface started and continued until the donor star reached four different values of the mass, $0.26, 0.28, 0.3, 0.5$ and $0.8M_\odot$. We applied two different (arbitrary) rates of the mass re-

Table 1. The parameters of the physical evolutionary models. The mass loss rate is in the unit of $10^{-9}M_\odot/\text{yr}$.

Model	M_2/M_\odot	R_2/R_\odot	T_{eff} [K]	L_2/L_\odot	M_c/M_\odot	$-\dot{M}$
A	0.28	13.3	4160	47.1	0.2530	0.85
B	0.30	13.6	4080	45.0	0.2504	1.56
C	0.50	16.1	3970	57.3	0.2550	5.33
D	0.80	18.9	4030	83.3	0.2656	13.0
E	0.90	19.6	4050	92.0	0.2703	16.0
F	1.00	20.3	4070	100.8	0.2720	19.5
G	1.40	22.8	4150	135.9	0.2834	37.7

moval, 1.3×10^{-9} and $1.3 \times 10^{-8}M_\odot/\text{yr}$. We found that the structure of the remnants was identical in both cases. Our motivation was to obtain thermal-equilibrium stars of a given mass. Since the structure of such stars does not depend on their evolutionary history, the prescription for mass removal from the surface was unimportant². Until then, the He core had not formed. The further evolution was followed at a constant total mass. The H-burning shell moves outwards, increasing the mass of the He core, M_c , and decreasing that of the H-rich envelope. Generally, this causes an increase of the radius of the stripped giant. However, when the mass of the remaining envelope gets sufficiently low, the giant starts to shrink, as shown in Fig. 4.

The results of our calculations are presented in Fig. 4, which show the evolutionary tracks in the core mass–radius diagram. The tracks are shown for the stripped giants of the masses equal $0.26, 0.28, 0.3, 0.5$ and $0.8M_\odot$. The stars evolve at constant mass and the driving mechanism is the progress of the H-burning shell moving outwards. The radii of the partially stripped giants generally increase with M_c , except for the shrinking when the masses of their envelopes become very low.

Fig. 4 show also values of the Roche-lobe radius of the donor calculated with the formula (3) for the assumed masses. Possible solutions that we consider as models for V1387 Aql are given by the intersections between a horizontal line (for a given mass) and the corresponding evolutionary track.

From Fig. 4, we immediately see that a stripped giant of the mass $0.26M_\odot$ cannot provide a solution since during its evolution it never attains a sufficiently large radius. We have checked that the same is true for the mass of $0.27M_\odot$. So, we are left with the remnants of the mass $\geq 0.28M_\odot$, which minimum value and its corresponding radius we show in Figs. 2 and 3. In further discussion, we shall consider remnants of the mass $0.28, 0.3, 0.5$ and $0.8M_\odot$. Magnified portions of the relevant tracks and horizontal lines from Fig. 4(a) are shown in Fig. 4(b). The possible solutions given by the intersections between the horizontal line (for a given mass) and the evolutionary track (for the same mass) are marked with consecutive capital letters, A, B, C and D for $M_2 = 0.28, 0.3, 0.5$ and $0.8M_\odot$, respectively, while the primed letters indicate the intersections during the final evolution stages.

² Fragos & McClintock (2015) suggested that this initial configuration could involve a donor star as massive as $5M_\odot$. The large amount of the mass from the donor accreted by black hole would then help to explain its claimed large spin. However, Fragos & McClintock (2015) assumed fully conservative mass transfer throughout the system history, which included epochs of highly super-Eddington accretion, during which strong outflows most likely took place, questioning that assumption.

We point out that the solutions A' and B' are unphysical as they do not assure a continuous mass transfer between the components of the binary system since solutions lie on the declining parts of the evolutionary tracks. During this evolutionary phase, the star shrinks with the growing mass of the core. Therefore, any mass outflow would be quickly stopped. The parameters of the physical solutions are given in Table 1, including their effective temperature and luminosity.

We note that the dependence of the stellar radius on the core mass can be considered for three different situations. First, we can consider the evolution of isolated giants at constant mass, as in Fig. 4. While this evolution does depend on the stellar mass, this dependence is relatively weak, and we can provide a fitting formula for the main dependence of $R_2(M_c)$ averaged over M_2 , as also done by WRS83. Then, we can consider $R_2(M_c)$ during the mass transfer via Roche-lobe overflow, i.e., with a simultaneous decrease of the donor mass. This gives usually steeper dependencies. It corresponds to considering also the second term in equation (1) for \dot{R}_2 of WRS83. Finally, we can consider $R_2(M_c)$ for our solutions, imposing the stellar radius equal to that of the Roche lobe of a given mass. This does not correspond to any evolutionary sequence, but just parametrises our results for $P = 33.85$ d. This, in turn, gives a flatter dependence.

We compare our radius vs. the core mass dependencies with the results of WRS83 (and of King 1993, who retained only the first order in their formulae). They correspond to the first case above, i.e., for evolution of an isolated star, and averaging over neglecting the dependence on M_2 . Given that we use different chemical composition and more contemporary physics (especially opacities), our results, while qualitatively similar, are quantitatively different. While WRS83 obtained $R_2 \propto M_c^{5.1}$, we find on average for $M_2 \geq 0.5M_\odot$,

$$R_2 \simeq 14R_\odot [M_c/(0.25M_\odot)]^{4.3}, \quad (7)$$

for the evolution of a giant at a constant mass. We do see some dependence on M_2 in Fig. 4, especially for low masses (see also Zdziarski et al. 2016). Also, this dependence excludes ranges of M_c close to M_2 , when the star starts to shrink. If we consider only the radii equal to the Roche-lobe radii at the period of GRS 1915+105 (the third case above), we find $R_2 \propto M_c^{5.2}$.

3.2 The radius–luminosity plane

So far, we have made use only of the value of the radius of V1387 Aql (which can be determined precisely for a given total mass using equation 3). A second parameter, luminosity, can be estimated only less precisely, given the range of the allowed effective temperatures, $L_2 = 4\pi R_2^2 \sigma T_{\text{eff}}^4$, where σ is the Stefan-Boltzmann constant, and we use the values corresponding to giants of the spectral classes K0 III–M0 III, $T_{\text{eff}} = 3690\text{--}4660$ K (Cox 2000). This uncertainty leads to the corresponding uncertainty of the luminosity estimate. The range of L_2 at a given R_2 corresponding to the adopted range of T_{eff} is shown in Fig. 5.

Our evolutionary model predicts the luminosity at any stage, and we compare the values corresponding to our solutions, see Table 1, with the above constraints in Fig. 5. We have found that all our solutions lie in middle of the allowed range, indicating a good agreement of our evolutionary calculations with the standard parameters of giants of Cox (2000), in spite of the reduction of the

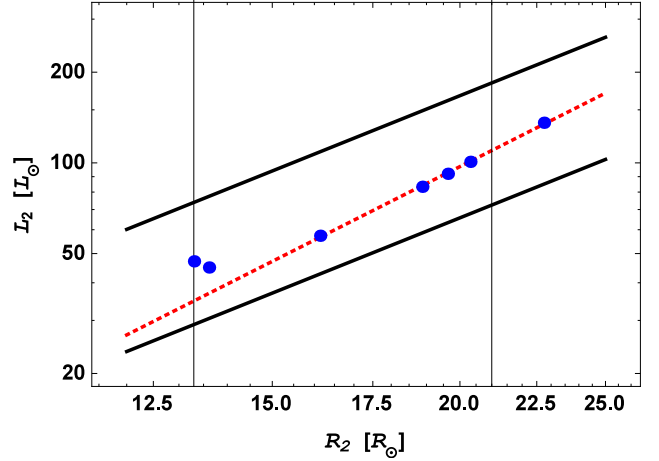


Figure 5. A comparison of our solutions with the observational constraints in the R_2 – L_2 plane. The heavy solid lines show the uncertainty range of L_2 due to the uncertainty of T_{eff} , and the vertical thin lines show the minimum radius of $13.3R_\odot$ (from our evolutionary calculations) and the maximum radius found to be allowed in Section 2. The blue points marked show the positions of the solutions A–G (in order of increasing R_2). The red dotted line shows the fit to the cases with $M_2 > 0.3M_\odot$ (solutions C–G).

mass due to accretion mass loss³. All of the solutions have the temperatures of $\approx 3990\text{--}4160$ K, which correspond to the spectral class of K5 III (Cox 2000). We thus find that the evolutionary considerations do not provide any significant upper limit on the mass and radius. For example, we have also calculated models with the final mass of $0.9M_\odot$ (solution E), $1.0M_\odot$ (solution F), and $1.4M_\odot$ (solution G), with the last one being well above the mass range allowed by the observations, and found that those solutions also lie in the middle of the range of L_2 allowed by the adopted range of T_{eff} . We show their parameters in Table 1.

One comment that should be made about our models concerns the luminosity of a star losing mass through Roche lobe overflow. If the mass outflow is very rapid, the surface luminosity of the star may become significantly lower than that without outflow (as noted by Greiner et al. 2001a). It is known that the black hole in the system is accreting matter roughly at the Eddington rate, $\sim 10^{-7}M_\odot/\text{yr}$, though the rate of the mass loss from V1387 Aql is much lower, see Section 4. However, we have found that even the Eddington rate is not high enough to decrease substantially the stellar surface luminosity. We superimposed a mass outflow at about Eddington rate on our model A, and found that the internal radiation flux in the outer layers started to decrease toward the surface, indicating that these layers were departing from thermal equilibrium. However, this departure was very small. The surface luminosity of the model with the outflow was smaller by less than 1 per cent compared with the model without outflow.

The obtained values of the luminosity show a similar steep dependence (excluding $M_2 = 0.28$ and $0.3M_\odot$) on the core mass to that of WRS83 of $L_2 \propto M_c^{8.1}$, but our normalization is ~ 50 per cent higher,

$$L_2 \simeq 50L_\odot [M_c/(0.25M_\odot)]^{8.15}, \quad (8)$$

³ We do not show here the solution A', which also agrees with above luminosity constraints. It was this solution that Ziółkowski (2015) advocated as the best model. Unfortunately, it was not noted at that time that this model did not assure a continuous mass transfer since it corresponded to the radius decreasing with time, and hence was unphysical.

with the relative error <3 per cent. Combining it with the dependence of R_2 assuming the Roche-lobe radius for the observed P (the third case at the end of Section 3.1), we find $L_2 \propto R_2^{2.5}$, which is shown in Fig. 5.

4 THE MASS OUTFLOW RATE FROM V1387 Aql

Having constructed the models describing the internal structure of V1387 Aql, we can calculate the rate of the mass transfer between the components of the binary system implied by our models. To do so, let us locate each of our models in a binary with $P = 33.85$ d and a $12.4M_\odot$ black hole. We assume the conservative mode of the mass transfer (conservation of the total mass and of the total orbital angular momentum). Then, we calculate numerically at which rate of the mass outflow from the star the changes of the stellar radius will follow the changes of the Roche lobe around it. The resulting rates are given in Table 1 and shown in Fig. 6, where we see a strong dependence of \dot{M}_2 on M_2 .

The results can be compared with the theoretical expression for \dot{M}_2 separated into three physical terms,

$$\dot{M}_2 = \left(\frac{dR_2}{dM_2} \right)^{-1} \frac{dR_2}{dM_c} \dot{M}_c, \quad (9)$$

where dR_2/dM_2 is the rate of the Roche-lobe changes with the changing mass, given by equation (12) of WRS83, with $R_2 \propto M_2^{-5/3}$ at $M_2 \ll M_1$, and dR_2/dM_c is the derivative along the solution with the mass transfer, i.e., that for the second case discussed at the end of Section 3.1. We find $R_2 \propto M_c^{c_1}$ along the solutions with the mass transfer, with, e.g., $c_1 \approx 4.71$ at $M_2 = 0.9M_\odot$ (and $c_1 \approx 4.53$ – 4.88 for $M_2 = 0.5$ – $1.4M_\odot$). The time derivative of the core mass is linked to the luminosity and the efficiency of hydrogen burning (accounting for neutrino losses), $\epsilon_H \approx 6.0 \times 10^{18}$ erg/g (as given by WRS83), $\dot{M}_c = L/(X'\epsilon_H)$. Here, X' is the H content immediately above the H-burning shell, which, due to the evolutionary H burning, can be substantially lower than the initial $X = 0.74$ (which still approximately equal that at the stellar surface). For example, $X' \approx 0.63$ for our case with $M_2 = 0.9M_\odot$ (and $X' \approx 0.62$ – 0.63 for $M_2 = 0.5$ – $1.4M_\odot$). We find the values of \dot{M}_2 obtained from equation (9) using the obtained values of c_1 and X' to agree very well with our numerical results, shown in Table 1 and Fig. 6. We note that $\dot{M}_2 \rightarrow 0$ at the exact minimum possible mass, because then $dR_2/dM_c \rightarrow 0$. Thus, arbitrarily low values of \dot{M}_2 can be obtained when the minimum allowed mass is approached, but this requires significant fine-tuning, see Fig. 4. We thus see that for the range of M_2 we have found to be allowed for GRS 1915+105, from 0.28 to $1M_\odot$, $-\dot{M}_2 \lesssim 2 \times 10^{-8} M_\odot \text{ y}^{-1}$.

We can compare our values with expressions given in literature. The rate given by equation (15) of WRS83 in terms of M_2 and M_c (and with a weak dependence on M_1) is completely equivalent to our equation (9), but we have now different numerical coefficients appearing in that formula. The formula (25a) in WRS83, giving \dot{M} in terms of M_2 and P (and M_1) is shown by the dashed line in Fig. 6. We see it has a different slope from that shown by our values. We have fitted the values of \dot{M} for $M_2 \geq 0.5M_\odot$, and obtained

$$-\dot{M}_2 \approx 7.4 \times 10^{-10} \left(\frac{P}{1 \text{ d}} \right)^{0.93} \left(\frac{M_2}{M_\odot} \right)^{1.9} M_\odot \text{ y}^{-1}, \quad (10)$$

where the dependence on P is kept unchanged with respect to WRS83. This is shown in Fig. 6 by the solid line. The disagreement at the lowest masses is a boundary effect, caused by $\dot{M}_2 \rightarrow 0$ at the exact minimum possible mass (as discussed above).

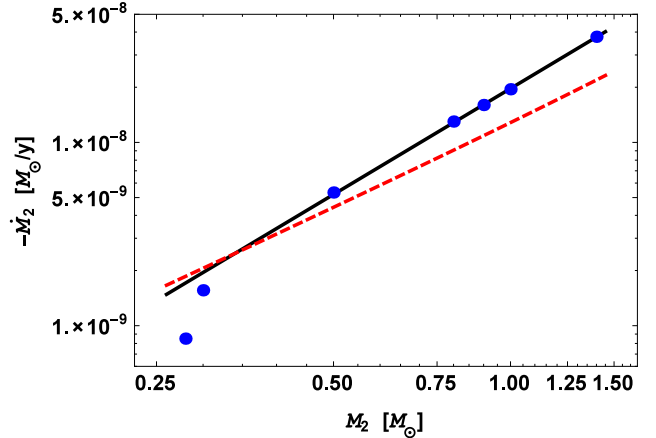


Figure 6. The mass transfer rate vs. the stellar mass. The blue dots show the rates obtained in our calculations, and the solid line shows the dependence fitted to the cases with $M_2 \geq 0.5M_\odot$, equation (10). The dashed line shows the dependence of equation (25a) of WRS83. The mass range allowed for GRS 1915+105 is $0.28 \leq M_2/M_\odot \leq 1$.

We can compare the obtained mass transfer rates with the average accretion rate required to power the outburst of GRS 1915+105. We used for that the results of Done, Wardziński & Gierliński (2004). From their fig. 5, we infer the average observed bolometric flux corresponding to $\sim 3/4$ of the Eddington luminosity for $M_1 = 14M_\odot$, pure H and at $d = 12.5$ kpc assumed by them, which is 7.1×10^{-8} erg cm $^{-2}$ s $^{-1}$. This corresponds to $L_1 \approx 6.2(d/8.6 \text{ kpc})^2 \times 10^{38}$ erg s $^{-1}$, and the accretion rate of $1.1(d/8.6 \text{ kpc})^2(\epsilon/0.1)^{-1} \times 10^{-7} M_\odot \text{ y}^{-1}$. We can compare our estimate of L with that of Vilhu (2002), which gives $L_1 \approx 5.7(d/8.6 \text{ kpc})^2 \times 10^{38}$ erg s $^{-1}$, a very similar value. We thus adopt $L_1 = 6(d/8.6 \text{ kpc})^2 \times 10^{38}$ erg s $^{-1}$.

At the observational best-fit donor mass value of $M_2 \approx 0.5M_\odot$ and at our corresponding value of \dot{M}_2 (Table 1), the duty cycle is about 5 per cent. The accreted mass during the 25 y of the outburst is $\approx 2.7(d/8.6 \text{ kpc})^2(\epsilon/0.1)^{-1} \times 10^{-6} M_\odot$. These values can be four times higher at the maximum allowed mass of $1M_\odot$, or much lower at the lowest allowed donor masses. See Truss & Done (2006) for estimates of the disc mass in GRS 1915+105.

We can compare our results with those of Vilhu (2002). He used the fits of WRS83 and considered the donor mass of Greiner et al. (2001b) as $M_2 \approx (1.2 \pm 0.2)M_\odot$. Thus, his best fit value of $-\dot{M}$ is $1.5 \times 10^{-8} M_\odot \text{ y}^{-1}$, which is comparable to our values at $M_2 \approx 0.8$ – 0.9 .

A potentially important effect we have neglected is the irradiation of the donor by the X-ray source (pointed out by Vilhu 2002). At the parameters at $M_2 = 0.5M_\odot$, the donor subtends a solid angle of $0.006 \times 4\pi$ (see equation 2), and the ratio of the irradiating luminosity (neglecting shielding and assuming isotropy) to $L_2/2$ (emitted by the hemisphere facing the black hole) is 33. At the estimated duty cycle, the average irradiating luminosity is larger than the intrinsic one, which may affect our estimates.

5 CONCLUSIONS

We have studied constraints on the present mass and radius of V1387 Aql by constructing evolutionary models of the internal structure of this star. We have compared the resulting radii and luminosity of our physical models to observational constraints. We

find solutions with stripped giants of the mass of $\geq 0.28M_{\odot}$ and of the spectral class K5 III, independent of the distance to the system, and a distance-dependent upper limit, $\lesssim 1M_{\odot}$. We have also obtained the constraints from the observed NIR magnitude of the companion, which are found to be consistent with the other constraints. Finally, we have estimated the mass transfer rate, which we found to be $\lesssim 2 \times 10^{-8}M_{\odot} \text{ y}^{-1}$. Comparing to the average luminosity of GRS 1915+105, we obtain the duty cycle of $\lesssim 20$ per cent. These two numbers are 4 times lower at $M_2 \simeq 0.5M_{\odot}$, which is the observationally-determined best-fit mass.

ACKNOWLEDGEMENTS

We thank Joanna Mikołajewska and Tomaso Belloni for valuable discussions. This research has been supported in part by the Polish National Science Centre grants 2013/10/M/ST9/00729 and 2015/18/A/ST9/00746.

REFERENCES

- Barnes T. G., Evans D. S., 1976, MNRAS, 174, 489
 Beer M. E., Podsiadlowski P., 2002, MNRAS, 331, 351
 Beuermann K., Baraffe I., Hauschildt P., 1999, A&A, 348, 524
 Cahn J. M., 1980, Sp. Sci. Rev., 27, 457
 Chapuis C., Corbel S., 2004, A&A, 414, 659
 Cox, A. N., 2000, Allen's astrophysical quantities, 4th ed., Springer
 Done C., Wardziński, G., Gierliński M., 2004, MNRAS, 349, 393
 Fender R. P., Garrington S. T., McKay D. J., Muxlow T. W. B., Pooley G. G., Spencer R. E., Stirling A. M., Waltman E. B., 1999, MNRAS, 304, 865
 Fragos T., McClintock J. E., 2015, ApJ, 800, 17
 Greiner J., Cuby J. G., McCaughrean M. J., 2001a, Nature, 414, 522
 Greiner J., Cuby J. G., McCaughrean M. J., Castro-Tirado A. J., Mennickent R. E., 2001b, A&A, 373, L37
 Harlaftis E. T., Greiner J., 2004, A&A, 414, L13
 Hjellming R. M., Rupen M. P., 1995, Nature, 375, 464
 Ingram A., Done C., 2011, MNRAS, 415, 2323
 Ingram A., Done C., Fragile P. C., 2009, MNRAS, 397, L101
 King, A. R., 1993, MNRAS, 260, L5
 Mirabel I. F., Rodriguez L. F., 1994, Nature, 371, 46
 Özel F., Psaltis D., Narayan R., McClintock J. E., 2010, ApJ, 725, 1918
 Paczyński B., 1967, Acta Astron., 17, 287
 Reid M. J., McClintock J. E., Steiner J. F., Steeghs D., Remillard R. A., Dhawan V., Narayan R., 2014, ApJ, 796, 2
 Steeghs D., McClintock J. E., Parsons S. G., Reid M. J., Littlefair S., Dhillon V. S., 2013, ApJ, 768, 185
 Truss M., Done C., 2006, MNRAS, 368, L25
 Vilhu O., 2002, A&A, 388, 936
 Wade R. A., Horne K., 1988, ApJ, 324, 411
 Webbink R. F., Rappaport, S. A., Savonije, G. J., 1983, ApJ, 270, 678 (WRS83)
 Wu J., Orosz J. A., McClintock J. E., Hasan I., Bailyn C. D., Gou L., Chen Z., 2016, ApJ, 825, 46
 Yan S.-P., Ding G.-Q., Wang N., Qu J.-L., Song L.-M., 2013, MNRAS, 434, 59
 Zdziarski, A. A., 2014, MNRAS, 444, 1113
 Zdziarski A. A., Gierliński M., Rao A. R., Vadawale S. V., Mikołajewska J., 2005, MNRAS, 360, 825
 Zdziarski A. A., Ziółkowski J., Bozzo E., Pjanka P., 2016, A&A, 595, A52
 Ziółkowski J., 2005, MNRAS, 358, 851
 Ziółkowski J., 2015, arXiv:1509.02819